Distribution Agreement

In presenting this thesis as a partial fulfillment of the requirements for a degree from Emory University, I hereby grant to Emory University and its agents the non-exclusive license to archive, make accessible, and display my thesis in whole or in part in all forms of media, now or hereafter now, including display on the World Wide Web. I understand that I may select some access restrictions as part of the online submission of this thesis. I retain all ownership rights to the copyright of the thesis. I also retain the right to use in future works (such as articles or books) all or part of this thesis.

Runming (Tony) Wang
March 22, 2023

Flexible Coordination Patterns of Rat Forelimb Motor Units Across Locomotion Speeds

By

Runming (Tony) Wang

Chethan Pandarinath, Ph.D.

Advisor

Neuroscience and Behavioral Biology

Chethan Pandarinath, Ph.D.

Advisor

Samuel Sober, Ph.D.

Committee Member

Gordon Berman, Ph.D.

Committee Member

2023

Flexible Coordination Patterns of Rat Forelimb Motor Units Across Locomotion Speeds

By

Runming (Tony) Wang

Chethan Pandarinath, Ph.D.

Advisor

An abstract of a thesis submitted to the Faculty of Emory College of Arts and Sciences

of Emory University in partial fulfillment of the requirements of the degree

of Bachelor of Sciences with Honors

Neuroscience and Behavioral Biology

2023

Abstract

Flexible Coordination Patterns of Rat Forelimb Motor Units Across Locomotion Speeds

By Runming (Tony) Wang

Background: The coordination of large motor unit (MU) populations during dynamic movements, such as locomotion, remains an area of inadequate understanding. While researchers have relied on Henneman's size principle for decades to understand the coordination pattern of MUs, several counterexamples of the size principle have been documented in intricate dynamic movements, revealing a more complex pattern of MU coordination. This study represents the first investigation into the flexible coordination of large MU populations across multiple dynamic behaviors.

Methods: This study conducted a comprehensive analysis of a dataset obtained from a rat named "Godzilla" on November 16th, 2022. The rats were trained to perform steady walking locomotion on an adjustable treadmill, and their kinematics were captured using a 3D motion tracking system based on DeepLabCut. Electrophysiological signals were recorded using novel intramuscular EMG arrays and were analyzed using functions within the rat-loco repository. State-space analysis was employed to visualize the coordination patterns of motor units across various speed conditions. The Kernel Density Estimation metric was used to estimate the similarity across MU responses, and the pairwise Euclidean distance between state-space trajectories was calculated to quantify significant differences between coordination patterns.

Results: The results of this analysis support the hypothesis that the adjustment in motor unit coordination is continuous rather than discrete. The state-space trajectories showed that the coordination patterns of motor units were flexible as the treadmill speed was adjusted, without significant discrete shifts. The OVL values also revealed that the similarity between the motor unit coordination patterns across speed conditions was high, indicating a flexible and continuous adjustment to changing force demands.

Conclusion: This study successfully analyzed kinematic and electrophysiological signals during treadmill locomotion tasks performed by rats, providing evidence for adaptive motor unit coordination patterns across varying speed conditions. The multi-faceted analysis approach utilized in this study emphasizes the importance of comprehensive analysis to fully understand the underlying mechanisms of motor unit coordination. Further research with additional datasets will be necessary to fully evaluate the transitions between coordination strategies.

Flexible Coordination Patterns of Rat Forelimb Motor Units Across Locomotion Speeds

By

Runming (Tony) Wang

Chethan Pandarinath, Ph.D.

Advisor

A thesis submitted to the Faculty of Emory College of Arts and Sciences

of Emory University in partial fulfillment of the requirements of the degree

of Bachelor of Sciences with Honors

Neuroscience and Behavioral Biology

2023

Acknowledgments

I would like to thank Dr. Chethan Pandarinath for the privilege of conducting research in his laboratory and for offering invaluable advice during my studies.

I would like to thank Sean O'Connell for his consistent and patient guidance over the past two years, which has been instrumental in my development as a researcher.

I would like to thank my loving parents, Jinyan Li and Xiaobing Wang, for their unwavering support, which has been my foundation throughout my academic pursuits.

Table of Contents

Abstract:

Background: The coordination of large motor unit (MU) populations during dynamic movements, such as locomotion, remains an area of inadequate understanding. While researchers have relied on Henneman's size principle for decades to understand the coordination pattern of MUs, several counterexamples of the size principle have been documented in intricate dynamic movements, revealing a more complex pattern of MU coordination. This study represents the first investigation into the flexible coordination of large MU populations across multiple dynamic behaviors.

Methods: This study conducted a comprehensive analysis of a dataset obtained from a rat named "Godzilla" on November 16th, 2022. The rats were trained to perform steady walking locomotion on an adjustable treadmill, and their kinematics were captured using a 3D motion tracking system based on DeepLabCut. Electrophysiological signals were recorded using novel intramuscular EMG arrays and were analyzed using functions within the rat-loco repository. State-space analysis was employed to visualize the coordination patterns of motor units across various speed conditions. The Kernel Density Estimation metric was used to estimate the similarity across MU responses, and the pairwise Euclidean distance between state-space trajectories was calculated to quantify significant differences between coordination patterns.

Results: The results of this analysis support the hypothesis that the adjustment in motor unit coordination is continuous rather than discrete. The state-space trajectories showed that the coordination patterns of motor units were flexible as the treadmill speed was adjusted, without significant discrete shifts. The OVL values also revealed that the similarity between the motor unit coordination patterns across speed conditions was high, indicating a flexible and continuous adjustment to changing force demands.

Conclusion: This study successfully analyzed kinematic and electrophysiological signals during treadmill locomotion tasks performed by rats, providing evidence for adaptive motor unit coordination patterns across varying speed conditions. The multi-faceted analysis approach utilized in this study emphasizes the importance of comprehensive analysis to fully understand the underlying mechanisms of motor unit coordination. Further research with additional datasets will be necessary to fully evaluate the transitions between coordination strategies.

Introduction and Background:

Movement is the only way we can physically interact with the world around us. All actions, from lifting a cup or brushing our teeth to the intricate dance of fingers across piano keys, necessitate the coordinated contractions of our muscles. Each muscle we have is controlled by motor units (MUs) that consist of an alpha motor neuron and thousands of muscle fibers it innervates (Heckman and Enoka, 2012; Bodine-Fowler et al., 1990). Despite the indispensable role that motor units play in upholding our physiological functionality, our understanding of the coordination of large MU populations across natural dynamic behaviors remains inadequate.

Researchers have relied on “Henneman's size principle” for years to understand the relationship between motor neurons and the muscle fibers they innervate. According to Henneman's size principle, motor units are recruited in order of their size, with smaller motor units being activated first, followed by progressively larger motor units as the force required for a task increases (Henneman, 1957; Henneman, 1965). Smaller alpha motor neurons control relatively fewer muscle fibers to form motor units that generate less force, while larger motor neurons control larger, more powerful motor units. These differences among various types of motor units were used to explain how the nervous system produces movements suitable for different situations (Hodson-Tole and Wakeling, 2009; Lai et al., 2018). In most instances, the small/slow motor units have lower activation thresholds than the larger units and are active during sustained effort activities (such as standing), while the large/fast motor units’ thresholds are reached during quick movements that require more force, such as jumping or running (Hennig and Lomo, 1985). As such, Henneman's size principle offers a valuable framework for understanding how motor units are recruited during muscle contractions to ensure efficient force production and minimize fatigue.

However, there are several potential limits to the size principle. Firstly, this fixed pattern was discovered over half a century ago, during which scientists were only capable of recording the activity of a limited number of motor units simultaneously (Henneman, 1957; Henneman, 1965). Secondly, subsequent MU research has predominantly concentrated on steady, isometric movement tasks, as opposed to more intricate dynamic movements, such as locomotion or knob-turning (Lai et al., 2018; Marshall et al., 2021). In fact, numerous studies conducted on multifunctional muscles have demonstrated counterexamples that reveal a shift in MU coordination towards earlier recruitment of larger MUs during rapid, dynamic behaviors (Hodson-Tole and Wakeling, 2009; Gollnick, 1974; Gillespie et al., 1974; Lee et al., 2013). Such time-shift counter-examples demonstrated that the coordination pattern of motor units is more complex and high-level than simply recruiting in order of their size (Marshall et al., 2022). Nevertheless, although these coordination shifts are well-documented, the precise mechanism underlying these changes remains an open question in the field. To develop a more comprehensive understanding of motor coordination, further in-depth studies of MU population coordination during dynamic movements are essential. Thus, a question arises: Is there a distinct transition in motor unit population coordination at a specific force output rate, or do the patterns of coordination change gradually and continuously across the force spectrum?

To fully assess and quantify the transition in motor unit coordination patterns, we decided to collect high-resolution electromyography (EMG) signals from rats' forelimbs while they are performing two distinct motor tasks, through the use of multiple-channel flexible intramuscular EMG arrays developed by the Sober Lab (Srivastava et al., 2017; Zia et al., 2018; Metallo et al., 2011). The first task involved treadmill locomotion with variable speeds and inclines, while the second task required the execution of forelimb knob rotation with variable torque conditions.

Since the locomotion task is mainly driven by central pattern generators located in spinal cords, while the knob rotation task is cortically dependent, both tests were designed to more comprehensively reveal the mechanism behind motor units' flexible coordination (Frigon, 2017; Drew et al., 2004; Pernia-Andreade et al., 2021; Lopez Ruiz et al., 2017)). The use of the novel flexible EMG array also allowed us to record multiple motor units simultaneously while the rats are performing intense motor tasks, which was something unachievable through previous experimental methods (Zia et al., 2018; Metallo et al., 2011). During my two years at the Systems Neural Engineering Lab, I have participated in animal training for both motor tasks. However, due to the extensiveness and complexity of this study, I will be only focusing on the experimental design, signal collection, and data analysis of the treadmill locomotion task in this honors thesis.

In the locomotion task, there are two main variables that determine the force demand of rats' forelimb muscles: speed and incline (Gillis and Biewener, 2001; Gillis and Biewener, 2002; Frigon, 2017). Thus, we decided to record rats' kinematics and forelimb EMG signals at a range of speed and incline conditions (5-20 meters/min, 0-20 degree incline). In this thesis, I will focus primarily on the effect of speed on rat forelimbs' motor unit coordination pattern. To accurately capture the three-dimension position of the rats' bodies while walking and running, we set up a four-camera motion-capture system and used various neural network pose estimation toolboxes, including DeepLabCut and Anipose, to measure the 3D position of rats' body parts at high frames-per-second (Mathis et al., 2018; Karashchuk et al. 2021). To record multiple MU activities simultaneously while rats were performing the locomotion tasks, we implanted 16-channel flexible arrays within rats' forelimbs. We specifically targeted three key muscles that

are heavily involved in locomotion and forelimb movement: Triceps Brachii, Biceps Brachii, and Acromiodeltoideus (Tosolini and Morris., 2012; Cohen and Gans, 1975).

Thanks to the high-channel count of our EMG recording, we were able to apply state-space analysis to measure the change of motor unit coordination across various speeds and inclines. This technique, more commonly used in cortical studies, allows researchers to study complex neural activity patterns through abstract trajectory representations (Feeney et al., 2017; Marshall et al., 2021; Grimby and Hannerz, 1977). This approach facilitates the interpretation of data and reveals underlying trends and patterns from population activity (Vyas et al., 2020). In this experiment, the state-space analysis method is able to produce individual trajectories for step cycles with various MU population coordination patterns, visualizing the separation and shift of MU coordination across various task conditions. Calculating the Euclidean distance between such trajectories enables us to quantify the significant difference between each coordination pattern. Calculating the probability density overlap of MU population response distributions also allows us to assess the similarity between MU coordination patterns across behavioral conditions (Chen et al., 2000; Fiorio, 2004).

We hypothesize that the MU coordination adjustment will be continuous, as opposed to discrete, across a range of force demands. This means there will be smooth and continuous changes in rats' forelimb MU coordination patterns as we gradually adjust the treadmill speed. By leveraging novel, state-of-art experimental and computational methods, the project seeks to provide valuable insights into how the nervous system flexibly adjusts motor unit coordination in dynamic behaviors. Since this is one of the first studies that focus on the flexible coordination of large MU populations across multiple dynamic behaviors, these insights could have important

implications for basic neuroscience research as well as for the development of neural interfacing technologies in the future (Ajiboye et al. 2017).

Methods:

Animal Training:

Four Long-Evans rats were trained weekly to perform steady walking locomotion on Columbus Instruments' adjustable Modular Treadmill at a range of speeds and inclines (Trained by Tony Wang, Sean O'Connell, Nevin Aresh, Mani Venkatesh, and Margo Shen). The treadmill speed was controlled by a treadmill controller at an accuracy of 0.1 meters per minute (Figure 1). The incline of the treadmill is adjustable in 5° increments, from 0 to 20 degrees, and its accuracy was verified using a digital angle meter (Figure 2, 3).

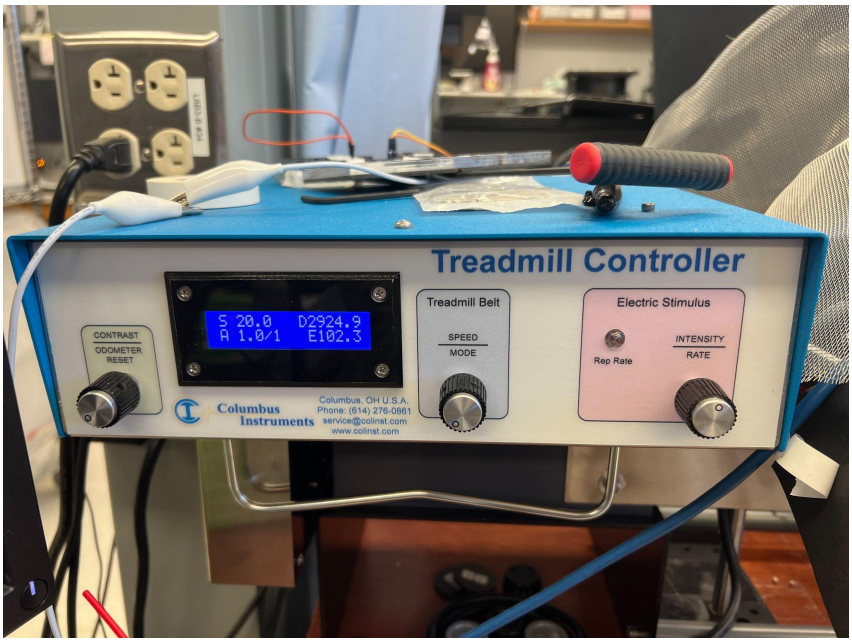

Figure 1. Treadmill Controller used to control speed.

Figure 2. Rat locomotion training treadmill set at incline 0.

Figure 3. Rat locomotion training treadmill set at incline 15.

To strengthen the locomotion performance of rats so that more kinematic data could be recorded after their implant surgeries, the training speed and trial counts were gradually increased as the rats became more adept in the locomotion task. To better manage and monitor the training progress of all rats, we also constructed a training spreadsheet that listed the current and target speed/duration/trial number for individual rats. Rats' performance was updated on the training calendar every week (Table 1). Due to our weekly locomotion training, we were able to record 24 minutes of kinematics recording (multiple 2-minute sessions for each condition) and 38 min of EMG recording at various inclines and speeds within two days after the surgery.

	A	B	C	D	E	F	G
1		Current Max Speed	Target Speed (training)	Target Speed (recording)	Current Trail * Duration	Target Trail * Duration	Recommended Training Speed
2	A	25	35	30	5 * 2 min	10 * 2 min	18, 24
3	B	25	35	30	5 * 2 min	10 * 2 min	18, 24
4	F	20	30	2*20, 4*15	2 * 1.5 min + 4 * 2 min	10 * 2 min	18, 24
5							
6	**New Rats**						
7	Hershey	10	20	20	5 * 1 min	10 * 2 min	6, 12
8	Inkblot	10	20	20	5 * 1 min	10 * 2 min	6, 12
9	Jellybean	10	20	20	3 * 1	10 * 2 min	6, 12
10	Kitkat	10	20	20	5 * 1	10 * 2 min	6, 12
11							
12							
13		Monday	Tuesday	Wednesday	Thursday	Friday	
14	H	✓			✓		
15	I	✓			✓		
16	J			✓		✓	
17	K			✓		✓	
18							
19		**Monday Jan 30**		**Friday Feb 3**			
20	**rat**	**speed**		**rat**	**speed**		
21	**1**	first time - 5		**Hershey**	Lot of turning around and wandering got up to 10 and seemed comfortable		
22	**2**	first time - 5		**Inkblot**	Got up to 10 speed slowly, looked very comfortable		
23	**3**	first time - 5		**Jellybean**	Liked to play and jump around a lot, looked very comfortable at 10 speed		
24	**4**	first time - 5		**KitKat**	Liked to play and jump around a lot, looked very comfortable at 10 speed (definetly the best new runner so far)		
25	Notes:	*all were frozen after treadmill off, hopefully next time they will have adapted		Notes:	*All but Jellybean(frozen for 30 secs) were "not-frozen" after this round of training They seemed to be a lot more comfortable with the treadmill enviornment		
26		5 mins			6-7 mins w/ breaks		

Table 1. Rat Locomotion Training Plan

Kinematics capturing:

The 3D motion tracking system consists of 4 FLIR Blackfly cameras (BFS-U3-16S2M-CS) that can capture monochrome videos up to 226 FPS. The cameras were

arranged circularly around the treadmill to reduce view obstruction and ensure triangulation. Black light-absorbing flocking cloths were also installed around the cameras and treadmill to remove reflective glares (Figure 2).

For our setup, all four cameras were controlled and synchronized by a Ubuntu Linux workstation with high-end gaming hardware. The synchronization and frame management across cameras were achieved by modifying the FLIR-Multicam GitHub repository to include a "trigger wait" state, which allowed an Arduino Uno to control frame capture of all cameras with a single square wave. To ensure the stability and consistency of frame capturing, we limited our video recording to 125 FPS and 720p resolution, which was sufficient of identifying the position of the rats' fingers while running (Figure 4).

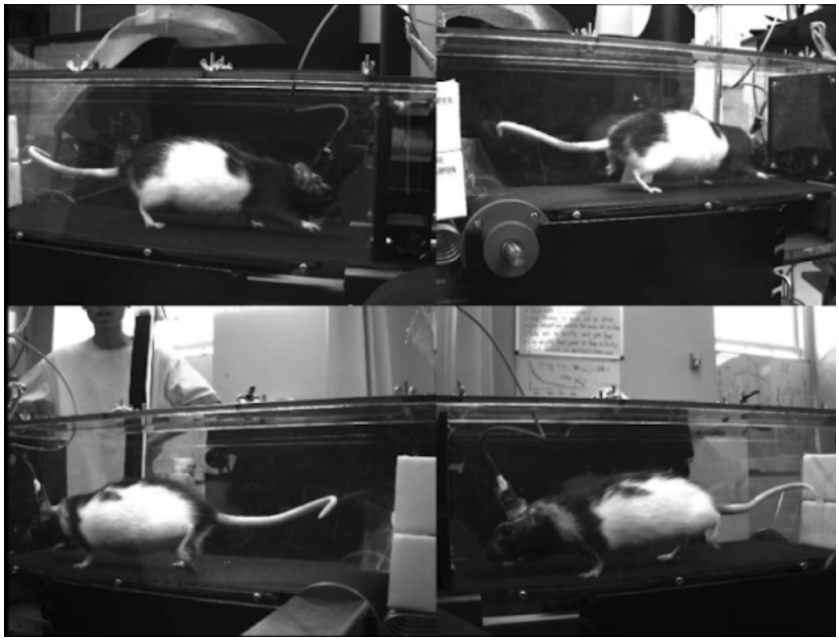

Figure 4. Synchronized video output of all four cameras.

The 3D position of rat forelimb joints was estimated and quantified using DeepLabCut (DLC), which is an open-source pose estimation toolkit based on convolutional neural networks (CNNs) that does not require the use of intrusive reflective markers (Mathis et al., 2018). DeepLabCut's strength lies in its ability to generalize well across different behavioral conditions. We specifically selected 10 body parts of rats for DLC training (rat's nose, tail base, and two joints on all four limbs), and manually labeled ~300 frames chosen randomly from recording sessions across all incline and speed conditions. After the DLC neural network training, we then used Anipose, a Python toolkit that is built on top of DLC, to automatically calibrate and triangulate body part positions across all 4 cameras (Karashchuk et al., 2021). Anipose triangulates the 2D key points obtained from DeepLabCut across multiple camera views to reconstruct the 3D pose. It also calibrates the cameras by determining their positions and orientations in the 3D space using a calibration object with known geometry. In our setup, we used a 5*8 ChArUco board to calibrate camera positions, and used three orthogonally positioned screws on the treadmill ceiling as the origin and reference to calculate the relative position of rats while running. This neural network tracking setup enabled us to consistently estimate the 3D position of all 10 body parts at various speeds and incline settings, with millimeter precision (Figure 5) (our latest DLC model, GeneralRat-Tony-2022-12-13 iteration 2, has a test pixel error of 2.69, estimated by DLC's built-in model evaluation function).

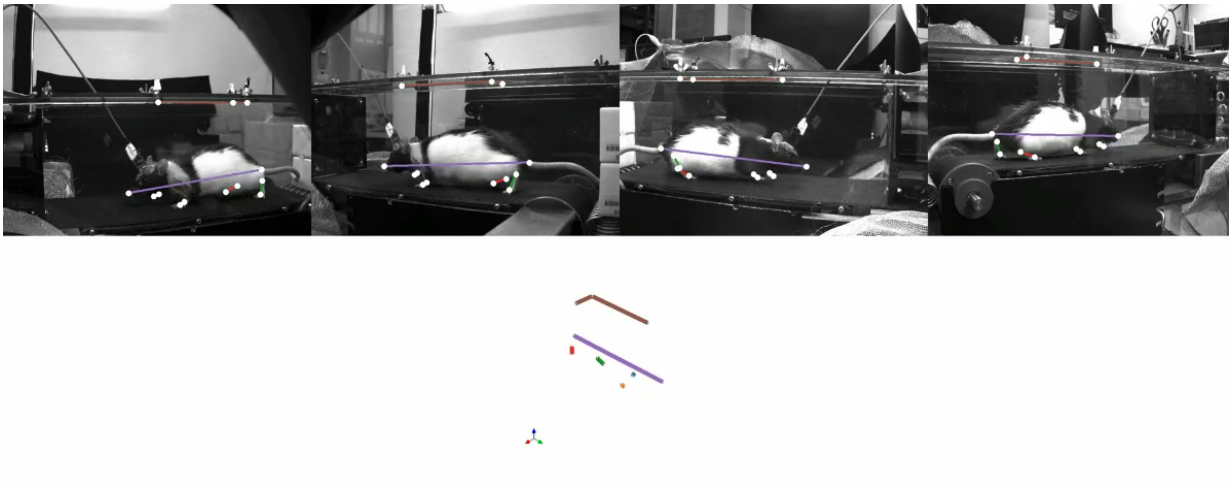

Figure 5. 3D position of rat body parts estimated by DLC and Anipose.

EMG Array Surgical Implantation:

The implantation procedure for collecting EMG data, performed by Sean O'Connell, begins with shaving and securing the rat before making incisions and inserting the flexible high-resolution 16-channel EMG array under the skin. After identifying the skull crest and Triceps location, a tunnel is created under the skin to thread the connector to the skull. Threads are then intramuscularly sutured onto the desired target muscles, such as the Triceps Brachii, Biceps Brachii, or Acromiodeltoidius. The arrays were inserted perpendicular to the forelimb muscle fibers to maximize the number of different motor units they can record. Next, the shoulder incision site is closed, and bone screws are implanted to secure the head cap. The connector and head cap is attached using dental cement, with care taken to ensure proper coverage and stability. Finally, all wounds are closed, and pain relief is administered to facilitate a smooth recovery for the animal.

We specifically targeted three key muscles that are heavily involved in locomotion and forelimb movement: Triceps Brachii, Biceps Brachii, and Acromiodeltoideus. Triceps Brachii opposes gravity during locomotion and posture, while the Biceps Brachii flexes and supinates the forelimb. Acromiodeltoideus rotates the humerus medially, contributing to locomotor patterns, posture, and target reaching. These muscles were able to exhibit diverse motor unit activation patterns across functions (Tosolini and Morris., 2012; Choi and Hoover, 1996; Cohen and Gans, 1975)

EMG recording and Spike Sorting:

Electrophysiology signals recorded from the implanted arrays were acquired using an OpenEphys Acquisition Board, which has shown a higher motor unit recording resolution and signal-to-noise ratio compared to our previously used Intan RHS Stim/Recording Controller. A SYNC squarewave was recorded along with 16 channels of EMG recordings (set up by Sean O'Connell), which ensured accurate synchronization between ephys and kinematics recordings. The accuracy of the synchronization was validated by aligning EMG and motion-tracking data recorded from real-life locomotion trials.

To improve the quality of EMG recording, we covered the knob box in Faraday caging and grounded the knob box and treadmill to lower the noise floor during recording. We also noticed using a DC power source for the 2 treadmill lights had a large impact on reducing the 60Hz noise (5-10x reduction).

The EMG activity was spike-sorted using two methods: thresholding and Kilosort. For the thresholding methods, spikes were categorized based on their amplitudes. This method was applied selectively to channels with distinct MU waveforms and consistent voltage amplitude

separation. Thresholds were set at 150uV, 500uV, and 1700uV, enabling raster plot visualization and step cycle modulation of MU activity. To compare MU activity across steps, spike times were phase-shifted based on the fraction out of 2π radians for the full step cycle. These phase-shifted spikes were then divided across 100 bins for “bin and count” visualization.

KiloSort improved upon the single-channel thresholding method by avoiding misidentification and misassignment issues. In KiloSort, an average spatiotemporal signature or "template" waveform for each MU is defined across multiple neighboring channels, allowing robust waveform detection and reliable MU spike isolation to be achieved (Pachitariu et al., 2016). Drift filtering for spatial adjustments is also provided by this technique, ensuring accurate spike times are maintained (Pachitariu et al., 2016). Once proper MU spike isolation is verified, a 10ms Gaussian window was used for smoothing. Lastly, Jonathan Michaels’s Kilosort PixelProcessingPipeline was used for refined motor unit sorting and merging, which modified the raw output of KiloSort so that motor unit clusters meet the defined statistical parameters and avoid refractory period violations.

Data Analysis:

The kinematic and electrophysiological data can be sliced, aligned, analyzed, and visualized using a range of functions within the rat-loco repository, which is primarily written by Sean O’Connell (Figure 6). Such plot types include “sort”, “bin_and_count”, “raster”, “state_space”, and “spike_motion_plot”. The sliced step cycles were determined by the Y-dimension peaks of the palm of the implanted limb, which enabled us to perform stepwise comparisons across trials and conditions. These functions will be applied in the results section and further explained in the discussion.

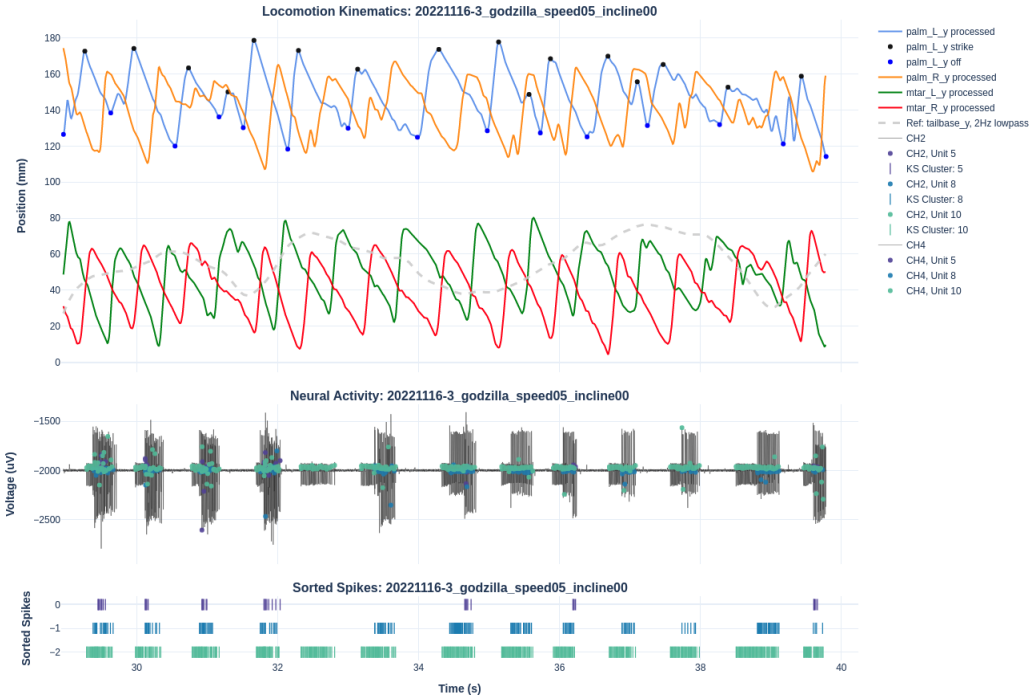

Figure 6. Visualization of kinematics and electrophysiology signals using rat-loco repo

In this thesis, a detailed examination of kinematics and electrophysiological signals will be conducted on the dataset obtained from the rat "Godzilla" on November 16th, 2022, which had 4 EMG threads intramuscularly implanted into its triceps brachii. The selected dataset exhibits superior electromyography (EMG) signal quality to date, as evidenced by a high signal-to-noise ratio (SNR > 200) for speeds of both 5 meters/minute and 10 meters/minute at incline 0 (Figure 7). Godzilla's recording consists of two 5m/min videos (sessions 3 and 7) and three 10m/min videos (sessions 5, 8, and 9), each 60 seconds long (7500 frames).

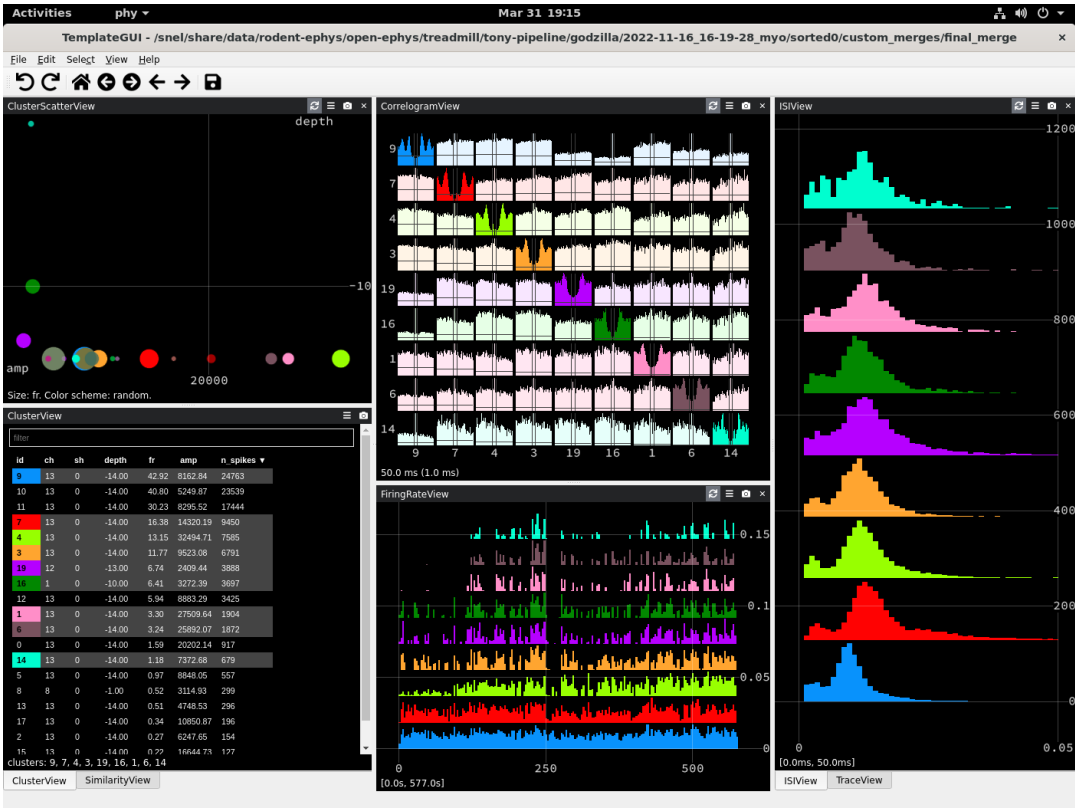

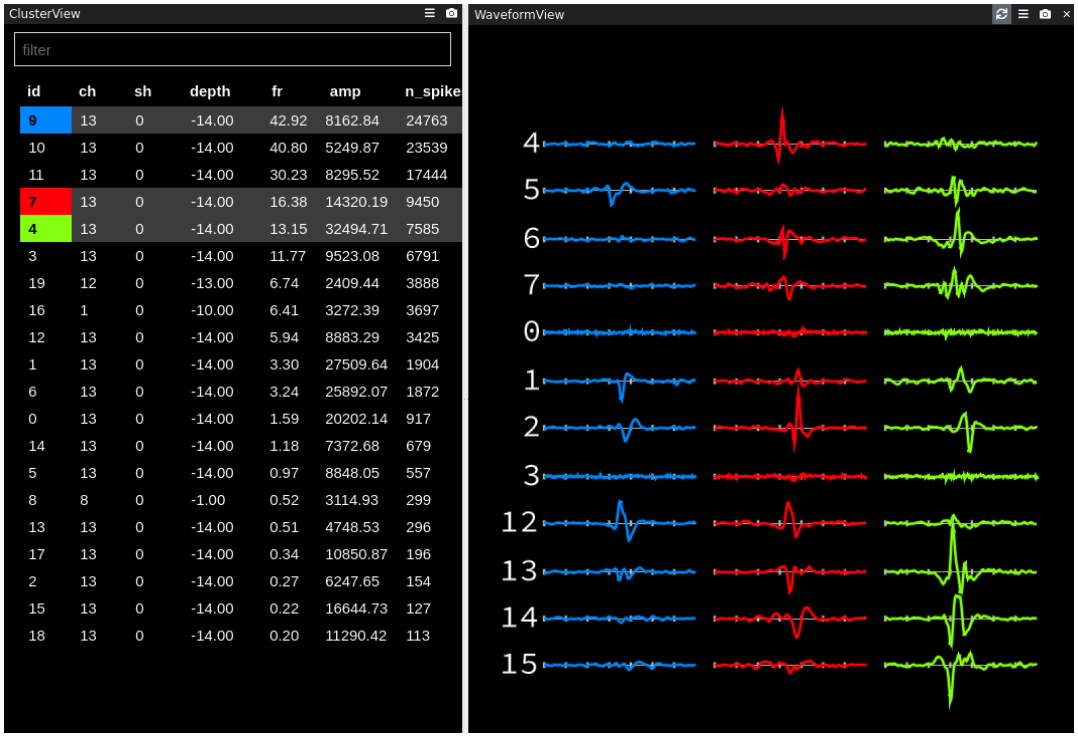

Figure 7. Selection of "good" motor unit clusters on Phy template GUI for Godzilla's recording

Using Phy's template GUI, merged motor unit clusters with a high number of spikes and good auto-correlation diagrams (minimal refractory period violations) were chosen for further analysis. For Godzilla's recording on Nov 16th, MU clusters with ID 10, 8, 5, 4, 20, 17, 2, 7, and 15 have been selected (in order of high to low spike counts) (Figure 7).

Since different combinations of bin width and Gaussian smoothing kernel width (sigma) can produce various shapes of state-space waveform patterns, we decided to set the bin width to 10ms and the number of radians binning to 100 for consistent representations. To determine whether there are discrete shifts in MU coordination across speed conditions, the Kernel Density Estimation (KDE) metric was applied to estimate the similarity across MU responses. Using the Overlap Coefficient (OVL), the probability density overlap between two MU response distributions can be calculated using the GitHub repository MUsim. If the OVL value is less than 5%, it can be concluded that the transition across speed conditions was not continuous. Pairwise Euclidean distance between state-space trajectories was also calculated to quantify the significant difference between coordination patterns at different speed conditions.

Results:

The analysis result will be presented in five parts: synchronization validation, binning and spike count analysis, state-space analysis, probability density overlap calculation, and Euclidean distance calculation. These results will provide evidence for the synchronization of EMG and motion-tracking data, visualize the binned motor unit activation patterns in phase-aligned step cycles, and calculate the OVL coefficient and geometric distance between state-space trajectories across speed conditions.

The analytical techniques and comparative methodologies employed in this thesis are readily adaptable for the assessment of data procured from incoming surgeries.

Synchronization validation:

Godzilla's recording on November 16th consists of two 5m/min videos (sessions 3 and 7) and three 10m/min videos (sessions 5, 8, and 9). As mentioned in the Methods section, MU clusters with ID 10, 8, and 5 exhibit the highest numbers of spikes with minimal refractory period violations when being analyzed in Phy's template GUI (Figure 7). Since the spike count is highest for cluster 10 and lowest for cluster 5, and the amplitude is highest for cluster 5 and lowest for cluster 10, we can infer that MU5 is the largest MU in size while MU 10 is the smallest. These three MU clusters were then used to generate a "sort" graph of session 3 using the rat-loco repository, which can verify whether the kinematics and electrophysiological data of Godzilla are in sync during locomotion (Figure 6). I specifically plotted the Y-dimension (vertical motion) of both palms and metatarsals (hind foot) of the rat to comprehensively visualize its gait pattern.

In Fig. 6, the ephys raster plot shows all three MU clusters were repeatedly activated during the stance phase of the locomotion, which is the phase where the rat's foot is in contact with the ground/treadmill and the limb is applying force to oppose gravity (indicated by the phase after palm_L_y strike and before palm_L_y off). During the swing phase, which begins when the foot first leaves the ground/treadmill and ends when the foot touches the ground again, all three MU clusters show little to no activation (Figure 6). Since Triceps Brachii is an extensor muscle and should be more activated during the stance phase, this activation pattern recorded by our EMG array is in sync with the kinematics of the rat.

Binning and spike count analysis:

To compare motor unit activation patterns across steps, spikes were phase-shifted based on the fraction out of 2π radians for the full step cycle. Phase shifting eliminated the consistency of time but it also allowed for more behaviorally relevant comparison because each step takes various amounts of time. These phase-shifted spikes were then divided across 100 bins for "bin and count" visualization.

In Figure 8, binned spike data was visualized for all 5 sessions of Godzilla's recording in order. Graphs for sessions 3 and 7 (speed 5) revealed lower spike counts for MU cluster 5 compared to graphs for sessions 5, 8, and 9 (speed 10). Additionally, slightly more MU 5 are activated earlier in speed 10 compared to speed 5 (figure 8). There does not appear to be a significant difference in MU activation timing between speeds 5 and 10 based on the binning graph. However, session 3's MU 5 was activated much slower compared to all other sessions (including session 7), with a much lower spike count.

Figure 8. Phase-aligned spikes binned into 100 bins (in the order of sessions 3, 7, 5, 8, and 9)

State-space analysis:

Due to the complexity of the neural activity, binning and spike counting of the acquired ephys signals are not sufficient of revealing the underlying patterns of motor unit coordination across speed conditions. Thus, state-space analysis was applied to all 5 recording sessions using rat-loco's "state_space" functions, which can produce 3D trajectories for individual step cycles.

In Figure 9, all trajectories (1 for each step) for each session were drawn in order. The overall trajectory clusters for speed 5 (sessions 3 and 7) appear to be more spread out than for speed 10 (sessions 5, 8, and 9), indicating a higher variance for MU coordination patterns across steps within the session. However, there does not appear to be a significant difference in overall shape or direction by looking at all trajectories at once. To better visualize the trajectory difference between plots, the mean trajectory of each session was plotted in Figure 10. The mean trajectories for all three speed 10 sessions appear extremely similar, with almost identical size, shape, and direction. The two speed 5 trajectories, on the other hand, reveal a dramatic difference in size. The session 7 trajectory is significantly shorter than the rest of the trajectories (with a noticeable difference in direction), and the session 3 trajectory is much more circular. The identically shaped trajectories between sessions 5, 8, and 9 indicate that the MU coordination pattern within the same speed condition is more similar than the coordination pattern across speed conditions.

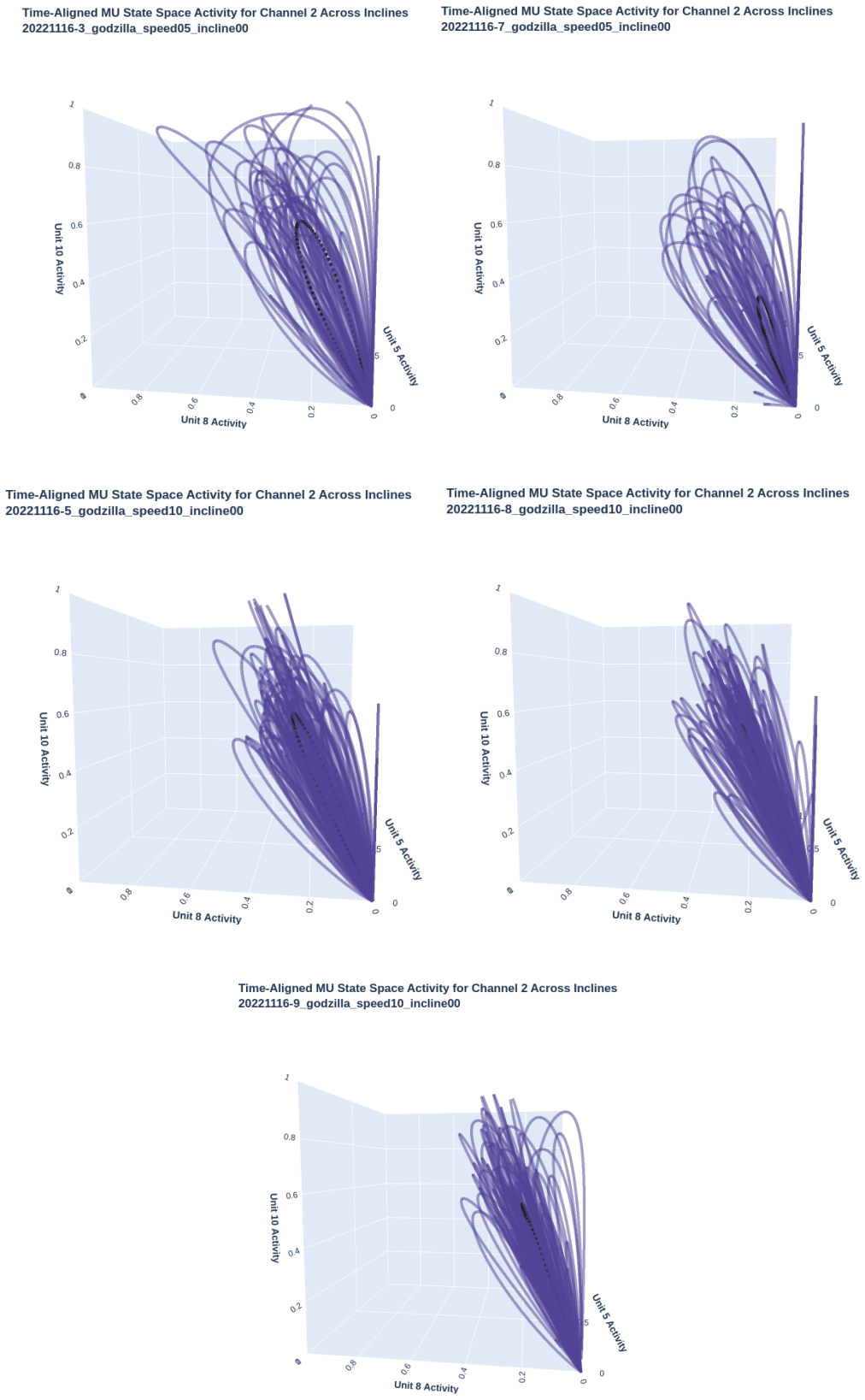

Figure 9. State-space trajectories for all step cycles (in the order of sessions 3, 7, 5, 8, and 9)

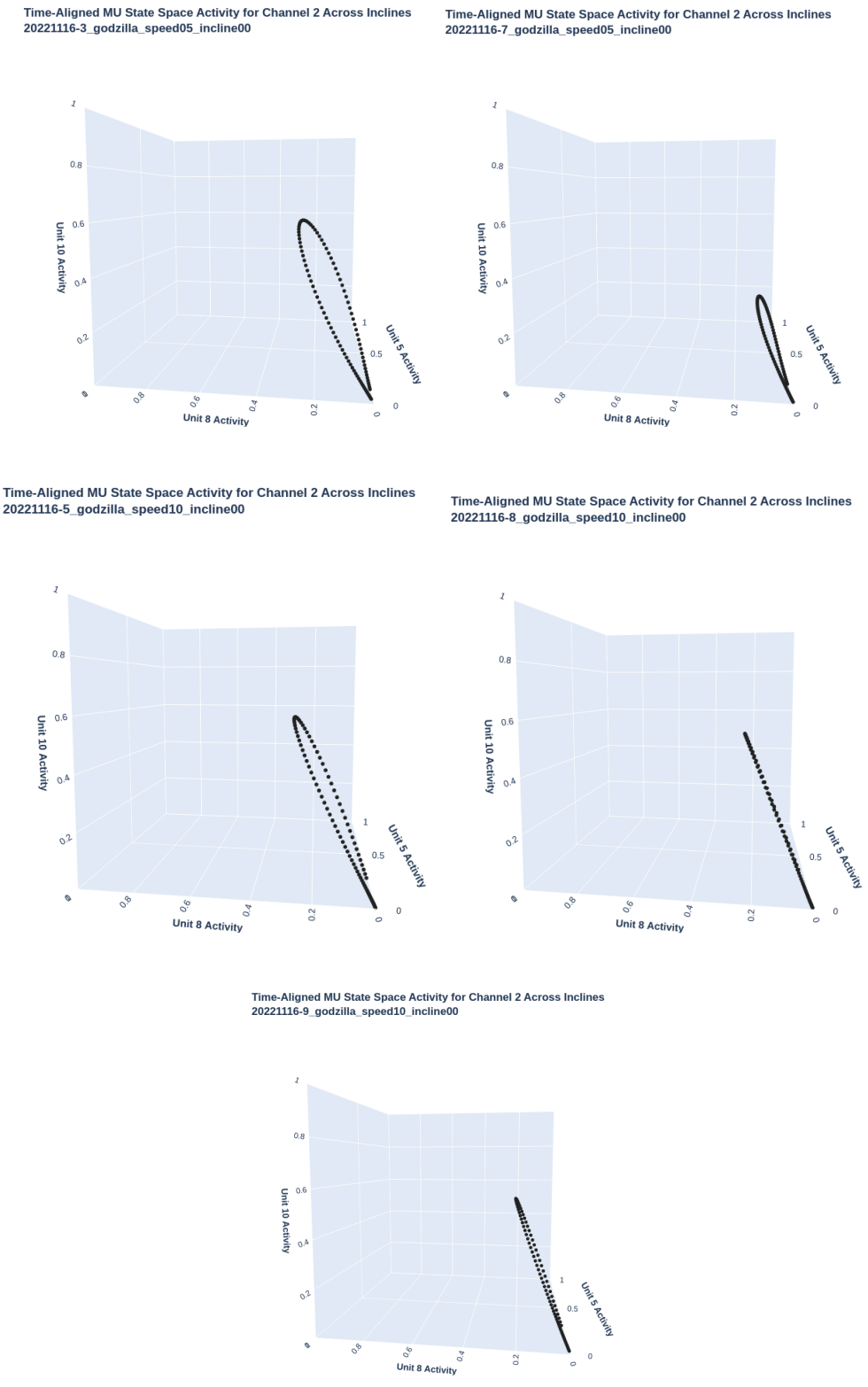

Figure 10. Mean state-space trajectory for each session (in the order of sessions 3, 7, 5, 8, 9)

Probability density overlap calculation:

Even though some differences between various sessions' MU coordination patterns can be observed through visualizing their state-space trajectories through a 3D plot, we still need a systematic way to quantify their difference. In this thesis, two quantification methods are proposed: probability density overlap calculation and pairwise Euclidean distance calculation.

To determine whether there are discrete shifts in MU coordination across speed conditions, the Kernel Density Estimation (KDE) metric was applied to estimate the similarity across MU responses. Using the Overlap Coefficient (OVL), the probability density overlap (OVL similarity values) across the trajectories of session pairs can be visualized using the GitHub repository MUsim (Figure 11). Since there are 5 recording sessions in total, 10 probability mass overlap amounts have been calculated.

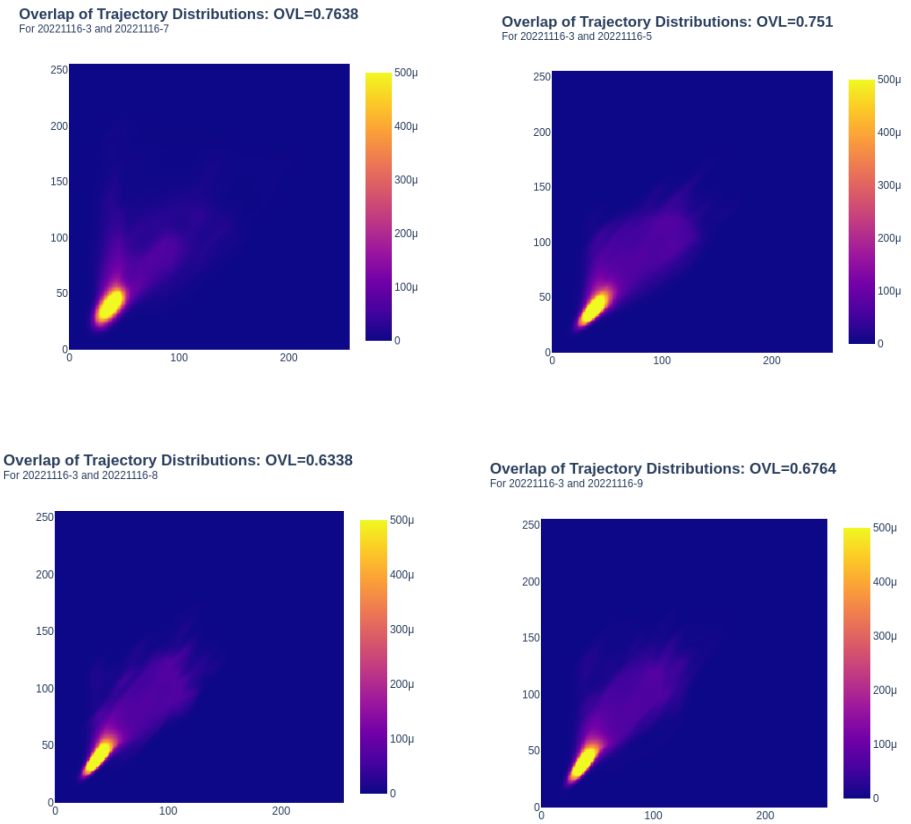

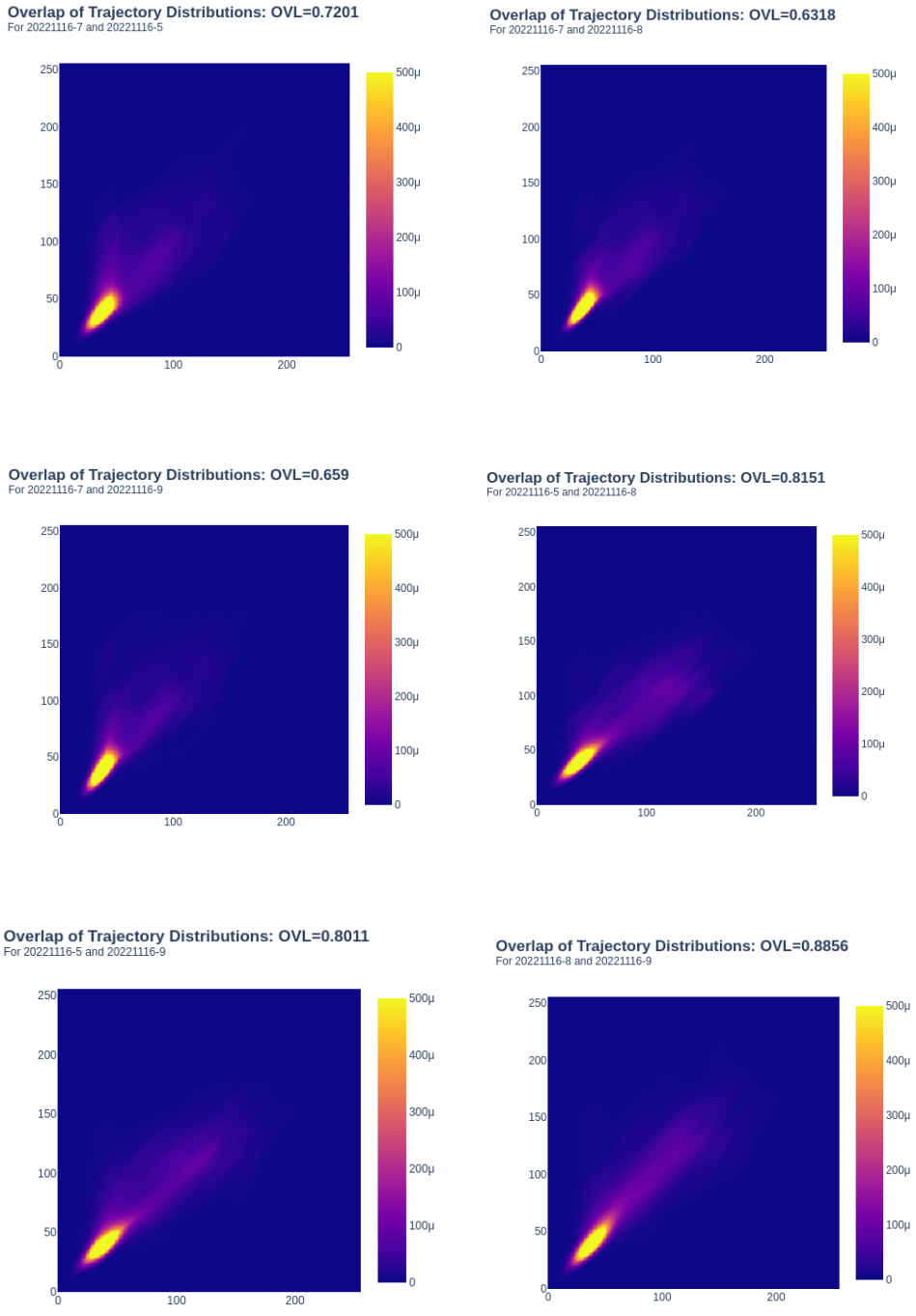

Figure 11. Probability mass overlap for all session-pairs

(in the order of sessions 3-7, 3-5, 3-8, 3-9, 7-5, 7-8, 7-9, 5-8, 5-9, and 8-9)

(3-7, 5-8, 5-9, and 8-9 are intra-speed comparisons while 3-5, 3-8, 3-9, 7-5, 7-8, 7-9 are inter-speed comparisons)

Here are the OVL results generated in order of permutations:

Session 3 - Session 7: 0.7638

Session 3 - Session 5: 0.751

Session 3 - Session 8: 0.6338

Session 3 - Session 9: 0.6764

Session 7 - Session 5: 0.7201

Session 7 - Session 8: 0.6318

Session 7 - Session 9: 0.659

Session 5 - Session 8: 0.8151

Session 5 - Session 9: 0.8011

Session 8 - Session 9: 0.8856

Among all session pairs, 3-7, 5-8, 5-9, and 8-9 are intra-speed comparisons while 3-5, 3-8, 3-9, 7-5, 7-8, 7-9 are inter-speed comparisons. Since all OVL values above are higher than 5%, it can be concluded that the MU coordination pattern transitions across speed were not discrete. However, to validate that there is in fact MU coordination flexibility between speed conditions, we also need to provide evidence showing OVL values for inter-speed comparisons are significantly different than that of the intra-speed comparisons.

Thus, a two-tailed t-test is conducted between same-speed OVL coefficients (SET1) and different-speed OVL coefficients (SET2):

t-value = (Mean_SET1 - Mean_SET2) / sqrt((Variance_SET1 / n1) + (Variance_SET2 / n2)) = (0.8164 - 0.6786) / sqrt((0.003187333 / 4) + (0.0053652 / 6)) = 0.1378 / sqrt(0.00079683325 + 0.0008942) = 0.1378 / 0.042244 = 3.2616

Degrees of freedom (df) = n1 + n2 - 2 = 4 + 6 - 2 = 8

Using a t-distribution table, we find the p-value to be around 0.011. Since the p-value (0.011) is less than the significance level (usually 0.05), we can reject the null hypothesis. This means that there is a statistically significant difference between the OVL for inter-speed comparisons and for intra-speed comparisons.

Euclidean distance calculation:

Euclidean distance between state-space trajectories was also calculated to quantify the significant difference between coordination patterns at different speed conditions. Instead of calculating the distribution distance between two sessions as a whole (seeing all state-space data points in one session as a single cluster), I decided to summate pairwise trajectory distances instead. Every trajectory in the first session is still being compared with every trajectory in the second session. However, for each trajectory comparison, only pairwise distances of points are summated in order. Since there will be the same number of binning in each trajectory (100 in this case), the pair-wise distance calculation does not require further non-linear mappings between the two datasets. Compared to cluster distance calculation, this method allows us to measure the trajectory shape differences between two sessions as time evolves.

Similar to the probability density overlap calculation, 10 summated pairwise Euclidean distances have been calculated in the order of permutations:

Session 3 - Session 7: 159645.079

Session 3 - Session 5: 136884.033

Session 3 - Session 8: 160760.526

Session 3 - Session 9: 154933.295

Session 7 - Session 5:	191138.845
Session 7 - Session 8:	207954.783
Session 7 - Session 9:	199582.354
Session 5 - Session 8:	169253.112
Session 5 - Session 9:	170174.776
Session 8 - Session 9:	191462.573

A step-wise summated distance curve has also been plotted for each session pair, with various speed conditions being colored differently (Figure 12). This curve provides a informative demonstration of how trajectories from two sessions differ as the step cycle progresses. From Figure 12, there does not appear to be a significant difference in pair-wise distances between session-pairs with different speeds and the same speeds.

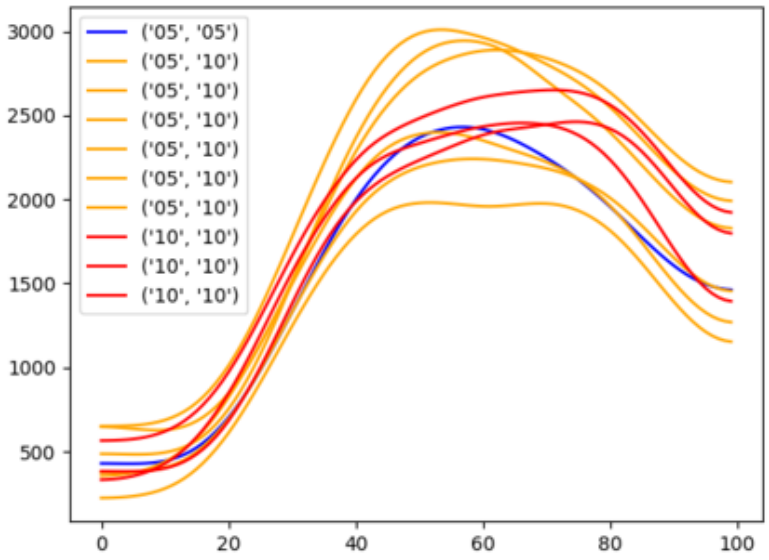

Figure 12. Step-wise summated distance curve for all session-pairs (in the order of sessions 3-7, 3-5, 3-8, 3-9, 7-5, 7-8, 7-9, 5-8, 5-9, and 8-9)

Similarly, a two-tailed t-test is conducted between same-speed session-pair distances (SET 1) and different-speed distances (SET 2). Using the same calculation steps as before, we found the t-value of the test to be 0.31025, with a p-value to be approximately 0.763. Since the p-value (0.763) is greater than the significance level (0.05), we fail to reject the null hypothesis. This means that there is no statistically significant difference between SET 1 and SET 2. In this case, there are no significant state-space distance differences between the inter-speed pairs and intra-speed pairs.

Discussion:

To our knowledge, this study represents the first investigation into the flexible coordination of large motor unit populations across multiple dynamic behaviors. Through the use of innovative hardware and software tools, our experimental setup offers a unique opportunity to comprehensively examine the activation patterns of numerous motor units while a rat performs various dynamic motor tasks (Zia et al., 2018; Metallo et al., 2011). Consequently, the findings of this study will offer valuable insights into fundamental neuroscience and neurotechnology research, regardless of the outcomes of our analysis (Ajiboye et al., 2017).

This thesis describes the recording and analysis of both kinematic and electrophysiological signals using our treadmill locomotion task setup. Additionally, an exemplary coordination pattern analysis is presented based on one of our many datasets, specifically, the recording of rat Godzilla on 11/16/2022. It should be noted that this analysis pipeline can be easily adapted to assess new data that we plan to record in the upcoming months, and that this specific thesis' results do not represent the entirety of our study. Nonetheless, as one of the highest quality EMG recordings we have obtained thus far, Godzilla's dataset has provided compelling evidence for the flexible coordination patterns of motor units across different speed conditions.

The results of the binning and spike count analysis reveal that step cycles at 5 meters/minute (particularly in session 3) have lower spike counts and slower activation for MU cluster 5 than those at 10 meters/minute. Using Phy's template GUI, we identified that MU cluster 5 has the highest number and lowest aptitude of spikes compared to the other two sorted MU clusters, indicating that MU 5 is the largest motor unit in size. This finding suggests that as speed increases from 5 to 10 meters/minute, the larger motor units are activated at an earlier

phase and a higher frequency. This result supports our hypothesis that during faster locomotion, the larger motor units are recruited earlier. Although the motor units from the Triceps Brachii of rat Godzilla do not demonstrate complete reversals in recruitment order relative to each other, they do show significant shifts in phase and activation intensity. To increase our confidence in the significance and reliability of these changes in motor unit coordination, further datasets involving more rats and conditions are necessary.

In the state-space analysis, the examination of both the overall trajectory cluster and the mean trajectory unveiled adaptive motor unit coordination patterns across various speed conditions. According to the size principle, if MU coordination remains constant, the trajectories from both speeds should adhere to the structure of a one-dimensional manifold. In this case, only the trajectory length would vary based on speed, with no discernible differences in shape or direction. Contrarily, as illustrated in Figures 9 and 10, the trajectories from session 7 displayed significant disparities in both direction and magnitude compared to other sessions. Furthermore, the trajectories from session 3 exhibited a more pronounced circular form. These variances in trajectories' shape and direction demonstrate that alterations in MU coordination patterns can be visually discerned through the state-space analysis method. Moreover, the strikingly consistent trajectory size, shape, and direction observed in all three sessions with speed 10 suggest that state-space analysis can reliably detect similar MU coordination patterns. This finding underscores the utility of state-space analysis as an effective method for investigating motor unit coordination patterns. With the acquisition of more data and the generation of additional trajectories from a diverse range of speed and incline conditions, our capacity to accurately and confidently evaluate the transition between coordination strategies will be enhanced. This will

enable us to determine whether these transitions are continuous or discrete in nature, thereby providing a more comprehensive understanding of the underlying coordination mechanisms.

Following the state-space analysis, we employed the distribution overlap method to quantitatively evaluate differences between motor unit coordination patterns across conditions. This method was performed pairwise for all recording sessions, resulting in a total of 10 probability mass overlap values, which were subsequently calculated and plotted. Although no conspicuous differences were observed between the overlap plots, the two-tailed t-test conducted for same-speed OVL values and different-speed OVL values yielded intriguing findings. Upon determining a t-value of 3.2616 and a p-value of 0.011, we ascertained that there is a statistically significant difference between the OVL amounts for inter-speed and intra-speed comparisons. This outcome furnishes robust, quantitative evidence supporting the notion that motor unit coordination patterns for distinct speeds can differ significantly from one another. Given that all OVL values exceed 5%, it can also be concluded that the MU coordination pattern transitions across speed were not discrete. Collectively, these results demonstrate that MU coordination is both adaptable and continuous across various speed conditions.

While the distribution overlap method provides strong evidence in support of our hypothesis, it is insufficient to fully capture the differences between state-space trajectories from two sessions. As the name suggests, the distribution overlap method focuses on calculating the overlap between trajectories, but it overlooks the shape and direction differences in non-overlapping regions of the trajectories. Consequently, we designed and applied the pairwise trajectory distance method to emphasize the significant differences in the time-evolving shapes of trajectories. In this specific dataset, the two-tailed t-test revealed that no significant state-space distance differences were observed between inter-speed pairs and intra-speed pairs. However,

this method could prove valuable for other datasets exhibiting more pronounced trajectory shape differences and more similar overall locations.

By comparing the results generated through binning and spike count analysis, state-space analysis, probability density overlap calculation, and Euclidean distance calculation, it is intriguing to discover that various visualization and quantification methods for motor unit (MU) coordination patterns may yield dramatically different outcomes. For instance, the difference between the coordination patterns of session 3 and the three speed-10 sessions is more apparent when employing the binning and spike count analysis, while the difference between the coordination patterns of session 7 and speed-10 sessions is more noticeable using state-space trajectory visualization. Additionally, although both probability density overlap calculation and Euclidean distance calculation are designed for quantitatively evaluating differences between MU coordination patterns across conditions, their t-tests produced entirely different results since they focus on distinct aspects of trajectory differences. Taken together, the findings from all methods offer a more comprehensive and multi-perspective analysis of MU coordination patterns. With the acquisition of more data and the generation of additional trajectories from a diverse range of speed and incline conditions, we are confident that we will be able to accurately and confidently assess the mechanisms underlying adaptive motor unit coordination.

Conclusion:

In conclusion, this study represents a pioneering investigation into the flexible coordination of large motor unit populations across multiple dynamic behaviors. Utilizing innovative hardware and software tools, we successfully recorded and analyzed kinematic and electrophysiological signals during treadmill locomotion tasks performed by rats, providing compelling evidence for adaptive motor unit coordination patterns across varying speed conditions.

Our multi-faceted analysis approach, which included sorting, binning and spike count analysis, state-space analysis, probability density overlap calculation, and Euclidean distance calculation, revealed the importance of a comprehensive analysis to fully understand the underlying mechanisms of motor unit coordination.

While our findings support the notion that motor unit coordination patterns are adaptable and continuous across various speed conditions, it is essential to gather additional datasets involving a greater number of rats and conditions to further substantiate these observations. As more data is acquired and additional trajectories are generated, we will be better equipped to accurately evaluate the transitions between coordination strategies, determining their continuous or discrete nature.

In summary, this thesis has laid a strong foundation for future research on adaptive motor unit coordination across diverse dynamic behaviors. As we continue to refine our experimental setup and analysis techniques, our findings will contribute to the advancement of fundamental neuroscience and neurotechnology research, ultimately improving our understanding of the complex mechanisms underlying motor unit coordination.

References:

Ajiboye, A. B., Willett, F. R., Young, D. R., Memberg, W. D., Murphy, B. A., Miller, J. P., Walter, B. L., Sweet, J. A., Hoyen, H. A., Keith, M. W., Peckham, P. H., Simeral, J. D., Donoghue, J. P., Hochberg, L. R., & Kirsch, R. F. (2017). Restoration of reaching and grasping in a person with tetraplegia through brain-controlled muscle stimulation: a proof-of-concept demonstration. Lancet Lond. Engl., 389(10081), 1821–1830. https://doi.org/10.1016/S0140-6736(17)30601-3

Bodine-Fowler, S., Garfinkel, A., Roy, R. R., & Edgerton, V. R. (1990). Spatial distribution of muscle fibers within the territory of a motor unit. Muscle Nerve, 13(12), 1133–1145. https://doi.org/10.1002/mus.880131208

Chen, Q., Wynne, R. J., Goulding, P., & Sandoz, D. (2000). The application of principal component analysis and kernel density estimation to enhance process monitoring. Control Engineering Practice, 8(5), 531–543. https://doi.org/10.1016/S0967-0661(99)00191-4

Cohen, A. H., & Gans, C. (1975). Muscle activity in rat locomotion: Movement analysis and electromyography of the flexors and extensors of the elbow. Journal of Morphology, 146(2), 177–196. https://doi.org/10.1002/jmor.1051460202

De Luca, C. J., & Erim, Z. (1994). Common drive of motor units in regulation of muscle force. Trends in Neurosciences, 17(7), 299–305. https://doi.org/10.1016/0166-2236(94)90064-7

Drew, T., Prentice, S., & Schepens, B. (2004). Cortical and brainstem control of locomotion. Progress in Brain Research, 143, 251–261. https://doi.org/10.1016/S0079-6123(03)43025-2

Feeney, D. F., Meyer, F. G., Noone, N., & Enoka, R. M. (2017). A latent low-dimensional common input drives a pool of motor neurons: A probabilistic latent state-space model. Journal of Neurophysiology, 118(4), 2238–2250. https://doi.org/10.1152/jn.00274.2017

Fiorio, C. V. (2004). Confidence Intervals for Kernel Density Estimation. Stata Journal, 4(2), 168–179. https://doi.org/10.1177/1536867X0400400207

Frigon, A. (2017). The neural control of interlimb coordination during mammalian locomotion. J. Neurophysiol, 117(6), 2224-2241. doi: 10.1152/in.00978.2016.

Gillis, G. B., & Biewener, A. A. (2001). Hindlimb muscle function in relation to speed and gait: in vivo patterns of strain and activation in a hip and knee extensor of the rat (Rattus norvegicus). The Journal of experimental biology, 204(15), 2717–2731. doi:10.1242/jeb.204.15.2717.

Gillis, G. B., & Biewener, A. A. (2002). Effects of surface grade on proximal hindlimb muscle strain and activation during rat locomotion. J. Appl. Physiol., 93(5), 1731-1743. doi: 10.1152/japplphysiol.00489.2002.

"GitHub-snel-repo/rat-loco: Functions for rat locomotion data processing and analysis." https://github.com/snel-repo/rat-loco (accessed Mar. 20, 2023).

"GitHub-snel-repo/MUsim." https://github.com/snel-repo/MUsim (accessed Mar. 20. 2023).

Gollnick, P. D., Piehl, K., & Saltin, B. (1974). Selective glycogen depletion pattern in human muscle fibres after exercise of varying intensity and at varying pedaling rates. J. Physiol., 241(1), 45-57. doi: 10.1113/jphysiol.1974.sp010639.

Grimby, L., & Hannerz, J. (1977). Firing Rate and Recruitment Order of Toe Extensor Motor Units in Different Modes of Voluntary Contraction. J. Physiol., 865-879.

Gillespie, C. A., Simpson, D. R., & Edgerton, V. R. (1974). Motor unit recruitment as reflected by muscle fibre glycogen loss in a prosimian (bushbaby) after running and jumping. J. Neurol. Neurosurg. Psychiatry, 37(7), 817-824. doi: 10.1136/jnnp.37.7.817.

Henneman, E. (1957). Relation between Size of Neurons and Their Susceptibility to Discharge. Science, 126(December), 1-3.

Henneman, E., Somjen, G., & Carpenter, D. O. (1965a). Functional Significance of Cell Size in Spinal Motoneurons.

Henneman, E., Somjen, G., & Carpenter, D. O. (1965b). Excitability and Inhibitability of Motoneurons of Different Sizes.

Heckman, C. J., & Enoka, R. M. (2012). Motor unit. Compr. Physiol., 2(4), 2629-2682. doi: 10.1002/cphy.c100087.

Hennig, R., & Lomo, T. (1985). Firing patterns of motor units in normal rats. Nature, 314(6007), 164-167. doi: 10.1038/314164a0

"Input/output manipulations with DeepLabCut - DeepLabCut." https://deeplabcut.github.io/DeepLab Cut/docs/recipes/io.html (accessed Mar. 20, 2023).

"JonathanAMichaels/PixelProcessingPipeline." https://github.com/smarkoco/PixelProcessingPipeline (accessed Mar. 20. 2023).

Karashchuk, P., et al. (2021). Anipose: A toolkit for robust markerless 3D pose estimation. Cell Rep., 36(13), 109730. doi: 10.1016/j.celrep.2021.109730.

Lai, A. K. M., Biewener, A. A., & Wakeling, J. M. (2018). Metabolic cost underlies task-dependent variations in motor unit recruitment. J. R. Soc. Interface, 15(148). doi: 10.1098/rsif.2018.0541.

Lee, S. S. M., De Boef Miara, M., Arnold, A. S., Biewener, A. A., & Wakeling, J. M. (2013). Recruitment of faster motor units is associated with greater rates of fascicle strain and rapid

changes in muscle force during locomotion. J. Exp. Biol., 216(2), 198–207. doi: 10.1242/jeb.072637.

Lopez Ruiz, J. R., Castro Velazquez, R., Roque-Rivera, A., Ramos-Murguialday, A., & Rivas Santos, V. M. (2017). Locomotion in intact and in brain cortex-ablated cats. Neuroscience, 358, 37-48. https://doi.org/10.1016/j.neuroscience.2017.06.026

Marshall, N. J., et al. (2022). Flexible neural control of motor units. Nat. Neurosci., 1–13. doi: 10.1038/s41593-022-01165-8.

Marshall, N. J., Glaser, J. I., Trautmann, E. M., Amematsro, E. A., & Sean, M. (2021). Flexible neural control of motor units.

Mathis, A., Mamidanna, P., Cury, K. M., Abe, T., Murthy, V. N., & Mathis, M. W. (2018). DeepLabCut: Markerless pose estimation of user-defined body parts with deep learning. Nature neuroscience, 21(9), 1281-1289. https://doi.org/10.1038/s41593-018-0209-y

Pachitariu, M., Steinmetz, N., Kadir, S., Carandini, M., & Harris, K. D. (2016). Kilosort: realtime spike-sorting for extracellular electrophysiology with hundreds of channels. bioRxiv, 061481. doi: 10.1101/061481.

Pachitariu, M., Steinmetz, N. A., Kadir, S. N., Carandini, M., & Harris, K. D. (2016). Fast and accurate spike sorting of high-channel count probes with KiloSort. Advances in Neural Information Processing Systems, 29.

Pernia-Andrade, A. J., Wenger, N., Esposito, M. S., & Tovote, P. (2021). Circuits for state-dependent modulation of locomotion. Frontiers in Human Neuroscience, 15, 745689. https://doi.org/10.3389/fnhum.2021.745689

“Setting up Anipose for 2D tracking - Anipose 0.8.1 documentation.” https://anipose.readthedocs.io/en/latest/start2d.html (accessed Mar. 20, 2023).

Srivastava, K. H., et al. (2017). Motor control by precisely timed spike patterns. Proc. Natl. Acad. Sci. U.S.A., 114(5), 1171–1176. doi: 10.1073/pnas.1611734114.

Tosolini, A. P., & Morris, R. (2012). Spatial characterization of the motor neuron columns supplying the rat forelimb. Neuroscience, 200, 19–30. doi: 10.1016/j.neuroscience.2011.10.054.

Vyas, S., Golub, M. D., Sussillo, D., & Shenoy, K. (2020). Computation Through Neural Population Dynamics. Annu. Rev. Neurosci., 249-275.

Wakeling, J. M., & Hodson-Tole, E. F. (2009). Motor unit recruitment for dynamic tasks: Current understanding and future directions. J. Comp. Physiol. [B], 179(1), 57–66. doi: 10.1007/s00360-008-0289-1.

Zia, M., Chung, B., Sober, S. J., & Bakir, M. S. (2018). Fabrication and Characterization of 3D Multi-Electrode Array on Flexible Substrate for In Vivo EMG Recording from Expiratory Muscle of Songbird. Tech. Dig. Int. Electron Devices Meet., 2018, 29.4.1-29.4.4. doi: 10.1109/IEDM.2018.8614503.